Available online at www.sciencedirect.com

SCIENCE DIRECT®

Cement and Concrete Research 35 (2005) 35–50

CEMENT AND CONCRETE RESEARCH

Influence of polymers on microstructure and adhesive strength of cementitious tile adhesive mortars

A. Jenni[a,*], L. Holzer[b], R. Zurbriggen[c], M. Herwegh[a]

[a]*Institute of Geological Sciences, University of Berne, Berne, Switzerland*
[b]*EMPA, Dübendorf, Switzerland*
[c]*Elotex AG, Sempach Station, Switzerland*

Received 9 July 2003; accepted 29 June 2004

Abstract

The impact of polymer modification on the physical properties of cementitious mortars is investigated using a multimethod approach. Special emphasis is put on the identification and quantification of different polymer components within the cementitious matrix. With respect to thin-bed applications, particularly tile adhesives, the spatial distributions of latex, cellulose ether (CE), polyvinyl alcohol (PVA), and cement hydration products can be quantified. It is shown that capillary forces and evaporation induce water fluxes in the interconnected part of the pore system, which transport CE, PVA, and cement ions to the mortar interfaces. In contrast, the distribution of latex remains homogeneous. In combination with results from qualitative experiments, the quantitative findings allow reconstruction of the evolution from fresh to hardened mortar, including polymer film formation, cement hydration, and water migration. The resulting microstructure and the failure modes can be correlated with the final adhesive strength of the tile adhesive. The results demonstrate that skinning prior to tile inlaying can strongly reduce wetting properties of the fresh mortar and lower final adhesive strength.

Keywords: Mortar; Microstructure; Polymers; Pull-out strength; SEM

1. Introduction

Commercially available tile adhesive mortars consist of a binder and mineral fillers, and are usually modified with cellulose ether (CE) and redispersible polymer powder (RP). These additives fulfil different tasks during the evolution from fresh to hardened mortar. The main purposes of CE are thickening, air entrainment, and water retention to establish proper workability properties. RPs further improve fresh mortar rheology, but mainly provide flexibility and tensile strength of the hardened mortar. The powder is usually manufactured by spray drying of a polyvinyl alcohol (PVA) containing latex emulsion. The most typical binder is ordinary Portland cement, used in combination with different types of mineral fillers. The simultaneous existence of binder and polymers provokes the interaction of two fundamental processes: polymer film formation and cement hydration. In comparison to common concrete technology, polymer-modified, thin-bed mortars are characterised by high water/cement ratios of about 0.8, but due to their high surface/volume ratios, they dry out more quickly. As a result, the cement has a low degree of hydration (less than 30%, instead of >90% as in concrete described in Ref. [1]). Tile adhesive mortars typically also contain a much higher air void content (25 vol.%, instead of <5% in concrete; see Fig. 1a).

To date, the influence of polymers has generally been investigated in an empirical manner by comparison of physical properties (compressive, flexural, and adhesive strengths) from different mortar formulations (e.g., Refs. [2–7]). In general, these studies document that the increase of strength can be correlated with concentration and type of

* Corresponding author. EPFL-STI-IMX-LMC, MXG-Ecublens, CH-1015 Lausanne, Switzerland. Tel.: +41 21 693 28 67; fax: +41 21 693 58 00.
E-mail addresses: andreas.jenni@epfl.ch (A. Jenni), lorenz.holzer@empa.ch (L. Holzer), roger.zurbriggen@elotex.com (R. Zurbriggen), marco.herwegh@geo.unibe.ch (M. Herwegh).

0008-8846/$ - see front matter © 2004 Elsevier Ltd. All rights reserved.
doi:10.1016/j.cemconres.2004.06.039

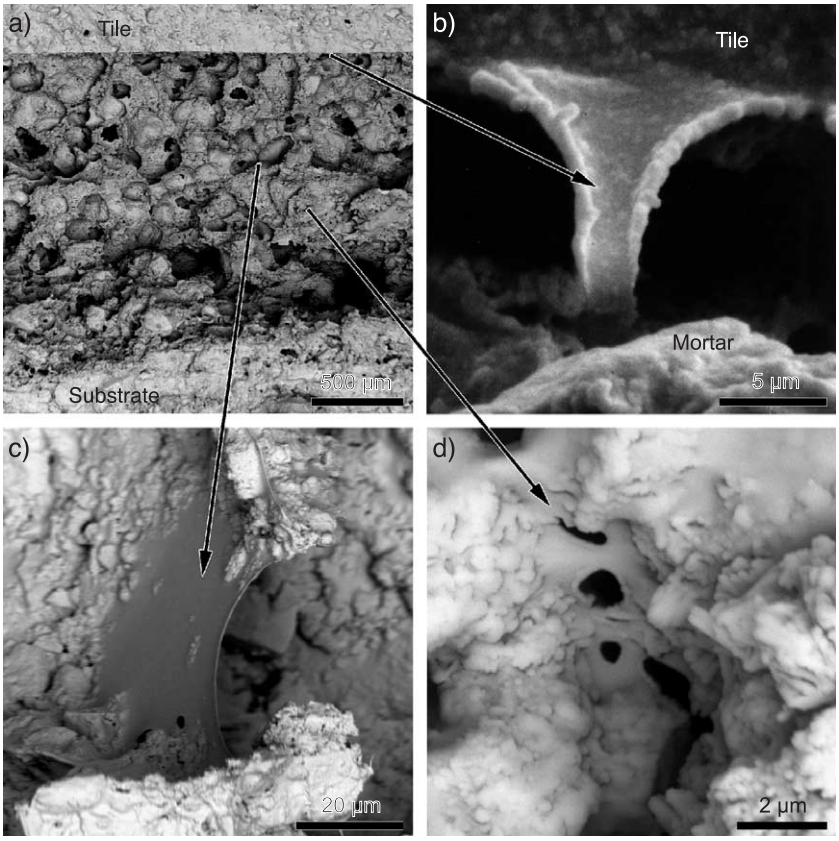

Fig. 1. SEM images showing the microstructure of a tile adhesive (fracture surfaces coated by Au evaporation technique). The mortar formulation is given in Table 1, but with 3 wt.% EVA redispersible powder. (a) Overview showing a cross-section through the mortar bed. The microstructure is typically dominated by a large number of air voids. Details: (b) latex film bridging a shrinkage crack at the mortar–tile interface. (c) CE film at the air void interface and (d) polymer film in a capillary pore of the cement–polymer matrix.

latex polymers. Furthermore, Larbi and Bijen [8] measured the pore solution chemistry of different polymer-modified mortar formulations in function of time, and concluded that latices interact with ions in pore solution. Changes in covalent latex bonds due to chemical interactions with cement ions are also documented by infrared spectroscopy [9,10]. A review of such interaction processes, mainly based on studies of ion measurements in aqueous systems, is given in Ref. [11].

In this paper, we focus on the fundamental relationship between the microstructure and the macroscopic properties of modified mortars. It is generally accepted that physical properties of cementitious materials are strongly dependent on microstructural aspects. For example, several studies correlate the pore size distribution with polymer modification (e.g., Ref. [12]). However, only few studies investigated the role of polymers in modified mortars as manifested by their morphology and distribution within the microstructure (e.g., Refs. [13,14]). Su et al. [15,16] and Dimmig [17] describe the adsorption of latex on cement grains immediately after mixing, resulting in early film formation and reduced hydration rates. The remaining part of the polymers, which is presumably dispersed in the pore water, undergoes film formation during the subsequent drying period.

In all microscopic investigations, the identification of polymers within the cementitious matrix is a major problem, especially for commercial formulations with low polymer concentrations of 1–4%. More severe, polymer modification of mortars generally are based on a variety of different polymer types, requiring the identification of these different phases in the mortar microfabric (various latices, CE, and PVA, the latter as a component in many commercial RPs).

For a profound understanding of the phase distributions in the mortar microstructure, which influence the physical properties of mortar thin-bed applications, the role of inhomogeneities has to be taken into account. Mortar–tile and mortar–substrate interfaces in particular represent inherent zones of weakness, which may dominate the final adhesive strength of the entire system. Further local inhomogeneities may form within the matrix by mechanical (e.g., application), physical (e.g., capillary forces/evaporation and associated water flux), or chemical processes (e.g., local precipitation). Water transport is a potential mechanism for efficient mass transfer, i.e., redistribution of dissolved chemical species. Schweizer [18] and Zurbriggen [19], for example, have documented enrichment and depletion of CE and inorganic phases at

mortar interfaces. In situ investigations in an environmental scanning electron microscope (ESEM) revealed that CE and PVA may become mobile during wetting and drying cycles, whereas latices remain immobile [20]. However, the general distribution patterns of these polymer types in thin-bed applications and the associated fractionation processes have not yet been described. For this purpose, the different polymer components and their spatial distribution within the mortar bed have to be visualised and quantified by different approaches [21,22]. In addition, the study of potential fractionation mechanisms during mortar evolution requires a time-resolved microanalysis. Unfortunately, it is impossible to continuously follow microstructure evolution in situ during the entire time ranging from fresh mortar stage to the final hardened mortar. Consequently, it is necessary to combine quantitative studies on the end product with in situ experiments to analyse a particular stage, and to trace critical periods of the microstructural evolution.

Until now, no straightforward method existed for microscopic identification and quantification of different polymer components within the mortar. The major goal of this study is to describe the general morphology of different polymer types within the mortar to distinguish them, to identify potential local enrichments, and to correlate them with the associated fractionation processes. The mutual interpretation of the microstructural evolution, mechanisms involved and resulting material properties, is an important step toward a better understanding of polymer–cement composites and the development of new products.

2. Materials and methods

The microstructural evolution of tile adhesives was investigated by a multitude of qualitative and quantitative methods, carried out (a) on the hardened mortar and (b) during transient stages of the mortar evolution.

(a) The general sample preparation resulted in a specimen composed of three layers, the concrete substrate, the mortar bed, and the tile. Depending on the analytical method used, specific preparation steps were performed. The film morphologies in hardened mortar were investigated by scanning electron microscopy (SEM) on fracture surfaces. Concentration profiles across the mortar bed were measured by wavelength dispersive X-ray spectroscopy (WDX) element mappings and fluorescence microscopy, both acquired on polished sections. Thermogravimetric and differential thermal analysis (TGA/DTA) of layer-wise sample series across the mortar bed resulted in the distribution pattern of portlandite and provided a rough idea on the spatially resolved degree of cement hydration.

(b) ESEM freeze–dry experiments on fresh mortar pastes revealed the CE behaviour during the early stages of mortar evolution. Light microscopy on polymer films in model systems outside the mortar illustrated principles of film formation mechanisms.

2.1. General sample preparation

With two exceptions (film formation experiments in model systems, and freeze–drying in ESEM), all samples were prepared according to EN 1348: the general mortar formulation was similar to commercial ceramic tile adhesives (Table 1), but not optimised to further improve the final mortar properties, e.g., adhesive strength. All dispersions are PVA stabilised. Furthermore, PVA is added as redispersing aid of the RP. This PVA is thought to be mobile in the mortar. All dispersions have a mean particle size $d(0.5)$ of about 1 μm. To identify the functionality of specific polymer types, formulations containing only one polymer type have also been investigated. In these samples, mineral fillers replaced the quantity of polymer omitted, and the percentages of all other components were kept constant.

After mixing, fresh mortar was applied on a concrete plate in two steps: as a first contact layer with a thickness corresponding to the coarsest grain size of the filler components (approximately 0.3 mm), which then was trowelled repeatedly with a toothed trowel (profiled 6×6×6 mm). After 5 min (Open Time), the fully vitrified ceramic tiles (5×5×0.5 cm) were laid in and loaded with 2 kg for 30 s. Then, the samples shown in Fig. 2 were stored for 28 days at 23 °C and 50% relative humidity (RH).

All results presented below are based on the chosen experimental setup and may deviate for different substrate and tile materials or dimensions (e.g., Ref. [18]).

Table 1
Typical formulation for ceramic tile adhesive used for all samples in this study, unless otherwise indicated

wt.% of dry mix	Component	Details
35.0	Ordinary Portland cement	CEM I 52.5 R, Jura Cement Fabriken, Wildegg, CH
40.0	Quartz sand	0.1–0.3 mm, Zimmerli Mineralwerke, Zürich, CH
22.5	Carbonate powder	Durcal 65, average grain size 57.5 μm, Omya, Oftringen, CH
0.5	Cellulose ether	MHEC 15000 PFF, Aqualon, Düsseldorf, D
2.0	Redispersible powder	VC (vinyl–acetate/ethylene/vinyl–chloride copolymer), SA (styrene/acrylic copolymer), EVA (ethylene/vinyl–acetate copolymer): laboratory samples with different latex compositions, containing PVA, Elotex, Sempach Station, CH
25.5	Water	Deionised

As common in mortar business, the percentages relate to 100 wt.% of the dry mix.

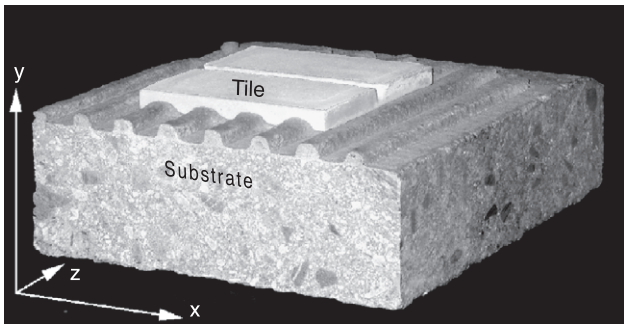

Fig. 2. The hardened mortar sample. Between tile and substrate, the mortar ripples are deformed to a continuous mortar layer, shown in Fig. 1a.

2.2. Light microscopy: film formation in model systems

Polymer films were produced outside the mortar using two different experimental setups: (a) film formation on metal grids and (b) film formation between two glass plates.

(a) As described in Refs. [23,24], films were produced from polymer dispersions/solutions using grids with 86×86 μm sized square voids (TEM grids), which were dipped into diluted polymer dispersions/solutions. The solid content of RP redispersions and of latex dispersions was about 10% in both cases, the solid content of CE solutions 2%, and of the PVA solutions 2.2%. This procedure resulted in the formation of films within the grid meshes. The polymer films contained holes (Fig. 3b), indicating a small film thickness, similar to the sail-like films observed at air void interfaces in mortars (Fig. 1). The polymer films were then investigated with transmitted light microscopy.

(b) Following the description of Ref. [25], agglomeration and film formation can be observed under the light microscope, where the polymer redispersion/solution or the fresh mortar paste is prepared between two glass slides. Due to evaporation, the waterfront retreats provoking the formation of polymer films between the glass slides parallel to the light beam (Fig. 3a and d). In case of PVA and CE, the optical anisotropy induced by polymer chain ordering causes birefringence colours, a clear indication for PVA and CE films.

2.3. Fluorescence laser scanning microscopy (LSM): PVA and CE distribution patterns

To visualise variations in the local distribution of PVA and CE, samples were formulated with only one specific

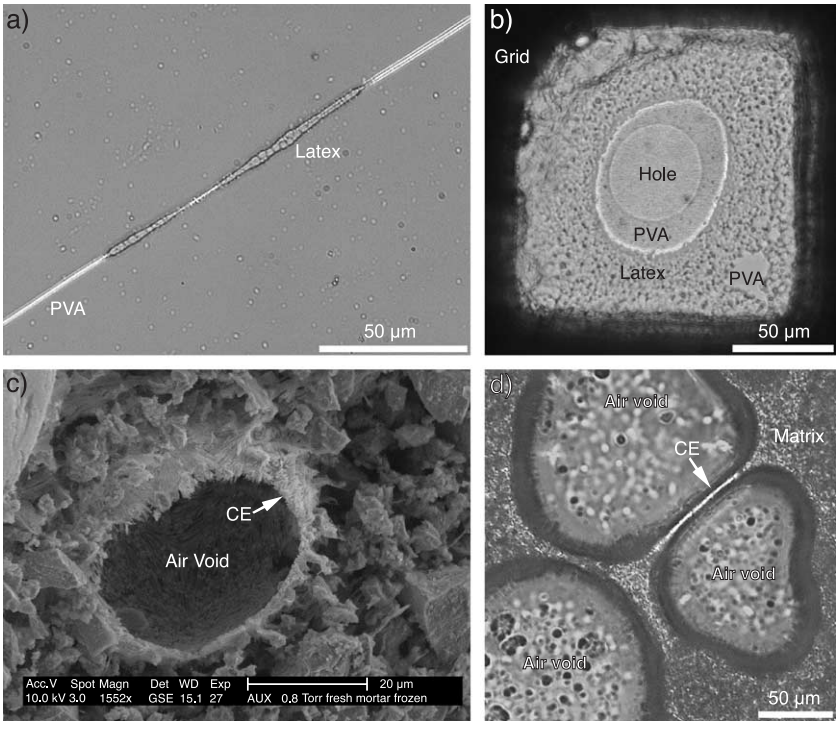

Fig. 3. Early polymer film formation in model systems (a, b) and in the fresh mortar (c, d). (a) Alternating sequences of polarising PVA (bright) and structured latex films formed at the evaporation front of a drying redispersion between two glass slides. The films formed parallel to the light beam of the microscope, perpendicular to the glass slides. (b) Top view (transmitted light microscopy) of a situation similar to (a), but formed in the void of a grid. There are clearly two phases formed, an inner PVA film (smooth), and an outer latex film (structured). (c) Fracture surface of a previously shock-frozen fresh mortar with an air void whose surface is covered with CE (water sublimated; ESEM in situ cryo-experiment). (d) Filler, CE, and water were mixed, applied as thin layer between two glass slides, and observed by polarisation light microscopy. Note that CE films were already formed between two air voids at the time of inspection, 15 min after mixing.

polymer being stained (either PVA or CE). Samples containing RP (latex+PVA) and stained CE, as well as samples containing latex, CE, and stained PVA were prepared according to Section 2.1. The hardened mortar samples were impregnated and polished [22] to obtain a mortar cross-section along the *xy* plane (Fig. 2). For subsequent investigations, a laser scanning microscope ZEISS 410 was used. Because PVA and CE did not occur within large voids or in the interior of unhydrated cement and filler grains, the resulting signals from the polymer were normalised to the area occupied by the cement–polymer matrix using digital image analysis. The cement–polymer matrix is defined as the total of all cement and polymer phases and gel/capillary pores [22]. In this manner, the polymer distributions in the cement–polymer matrix were obtained. Due to this normalisation, an eventual inhomogeneous distribution of air voids and fillers did not affect the polymer distribution. Variations of PVA and CE concentrations as a function of the distance from the substrate interface were obtained by segmentation of the LSM image into horizontal stripes oriented parallel to the aforementioned interface and lying in the *xy* plane (Fig. 2). The substrate was analysed with the same methods. An extensive description of polymer staining, sample preparation, sample measuring, image processing, quantification, and calculation of errors is given in Ref. [22].

2.4. Electron microscopy

2.4.1. Qualitative SEM investigations of polymer films on fracture surfaces

Fracture surfaces of mortar samples were investigated using a CamScan CS4 scanning electron microscope equipped with a Robinson backscattered electron (BSE) detector and a Voyager 4 digital image acquisition system for energy dispersive spectroscopy. Samples were coated by evaporation either with carbon or with gold (C: Balzers Carbon Coater; Au: Edwards E12E2). Distance between target and sample was around 25 cm. It is important to note that evaporation coatings with smaller distances can heat up the sample considerably and may destroy the polymer structures.

Polymer structures in the mortar microstructure are characterised by smooth surfaces. Unfortunately, this observation is also valid for cement gels, requiring additional identification criteria for polymer microstructures:

- Polymers have a much lower average atomic number (Z) compared to mineral components. The backscattering coefficient and the grey value on BSE images is a function of the Z value [26]. Therefore, polymer microstructures are transparent or dark on BSE images, in contrast to mineral phases, which have a significantly higher Z value. The comparison between BSE and secondary electron (SE) images is thus a reliable way to distinguish between polymer films and cementitious gels.
- Polymer phases are prone to be damaged under the electron beam [27] whereas gel-like mineral phases are much more resistant. Structural changes due to beam interactions can thus be used as criteria for the distinction between polymer and mineral components. Structural changes on the surface of polymer films in carbon-coated or in noncoated samples, e.g., in an ESEM, can be induced using high magnification, acceleration voltage, and beam current as well as an extended dwell time.

2.4.2. ESEM freeze–dry experiments on fresh mortar

To study the distribution of CE in fresh mortar, pastes with CE as the only polymer component were used (see Section 2.1 and Table 1). Immediately after mixing, small pieces of the fresh paste were shock frozen in liquid nitrogen. Fracture surfaces of shock-frozen samples were then studied in an ESEM-FEG XL30. The sample was inserted under the presence of liquid nitrogen into the sample chamber, where the liquid nitrogen was evaporated and the sublimation of the frozen pore solution was followed using N_2 as imaging gas. After sublimation of the pore solution, distribution of CE in fresh mortars became visible (Fig. 3c). Polymer and mineral phases were distinguished according to the criteria given above.

2.4.3. Latex distribution patterns based on WDX element mapping

VC latex contains chlorine, which allowed the localisation of this latex type by chlorine mapping done by WDX. Element distribution maps were measured on impregnated and polished samples using an electron microprobe (Cameca SX-50). The mortar formulation is given in Table 1. Similar to CE and PVA quantification, an identical normalisation procedure was applied to the element distribution maps to obtain the VC latex distribution in the cement–polymer matrix. The complete description of sample preparation, data acquisition, image processing, quantification, and calculation of errors is given in Ref. [22]. The substrate was analysed by the same method. Ca, Si, and BSE were mapped simultaneously with Cl. Calcium and Si mappings were used to discriminate and quantify calcite and quartz fillers, air voids, and the cement–polymer matrix. In addition, anhydrous clinker was distinguished from the rest of the matrix based on BSE images. According to Ref. [28], the fraction of anhydrous clinker was used as a measure for the degree of hydration.

2.5. Thermogravimetric analysis

In general, the samples were prepared and measured after Ref. [19]. More specifically, the tile (5×5 cm) was removed from the hardened sample after a normal dry storage following Section 2.1 (formulation according to

Table 1). To receive a plane failure surface at the tile–mortar interface, a polyethylene foil was inserted between tile and mortar. A zone of about 1.5 cm width was then removed from the mortar rim to avoid carbonation artefacts from the mortar edges, leaving a quadratic analysis region of 2 cm length and about 1.4 mm height. Sequential profiles through the analysis volume were obtained by scratching of layers of 0.2 mm thickness using a variety of distance holders. Each layer was measured by TGA on a TGA/SDTA 851^e from Mettler Toledo. The following experimental parameters were used: 150 μl platinum crucible, 30–1000 °C, 10 °C/min, 50 ml air/min. The use of air as circulation gas during measurement and the release of CO_2 by polymer decomposition as described in Ref. [29] may result in carbonation of $Ca(OH)_2$. This presumably leads to a systematic reduction of the measured $Ca(OH)_2$ concentration. However, taking into account this systematic error, the observed relative variation across the mortar bed can be considered to reflect true variations of the $Ca(OH)_2$ contents although the values of the absolute concentration are underestimated.

Based on the weight loss of the endothermic dehydration step at about 450 °C, the $Ca(OH)_2$ was stochiometrically quantified. The $Ca(OH)_2$ concentrations of each layer were then plotted vs. the vertical distance. Any fine-grained component is part of the cement matrix, which is enriched towards both interfaces: the tile and the substrate. To check for potential fractionations within the matrix, the quantity of the component has to be normalised with respect to the matrix. For this purpose, the measured values are normalised by the weight of fine filler and cement, where the amount of carbonate fine filler is estimated by thermal decarbonation between 550 and 800 °C. Using the formulation percentages (22.5 g $CaCO_3$ on 35 g of cement), a bulk weight of fine filler and cement was calculated. The required assumption that both fine filler and cement are homogeneously distributed throughout the matrix was confirmed by element mapping.

Furthermore, TGA allows an estimation of the degree of cement hydration. Most dry stored tile adhesives of test samples show a total dehydration weight loss indicating a water/cement ratio of 0.12. Assuming a minimum water/cement ratio required for full cement hydration of about 0.38 [30], the TGA data indicate that only about one third of the cement is hydrated.

2.6. Adhesive strength tests and failure surface analysis

The adhesive strength was measured on substrate–mortar–tile systems by standard tensile tests according to EN 1348. The errors based on the standard deviations are in the range of ±10%. The structure of the failure surface was then macro- and microscopically investigated. Most surfaces showed criteria of mixed adhesion and cohesion fracturing. In a first approach, macroscopic images of the failure surface on the tile side were acquired by a common colour flat bed scanner (Paragon Mustek 1200 A3 PRO). The area percentages of adhesion and cohesion failure were evaluated by image analysis (failure mode distribution after Ref. [7]). Due to the strong colour contrast between the light tile and dark mortar, adhesion and cohesion fractures were easily distinguished. The microstructure of the failure surface from tile and substrate are investigated by SEM in the same manner as described for fracture surfaces.

3. Results

3.1. Appearance of polymers in model systems

Investigations on polymers in simplified model systems, e.g., latex films outside the mortar, are generally straightforward in terms of preparation and reveal time-dependent information about redispersion and film formation. Fig. 3a shows a cross-section of alternating latex and PVA segments formed from a redispersion (redispersed RP) between two glass plates during water evaporation. The optical resolution was insufficient to study the presence of unordered PVA within or on the latex film. Fig. 3b shows latex and PVA films that formed due to drying of the redispersion on a grid.

Whereas latex and PVA form at the evaporation front that moves within the mortar from substrate to tile during hardening, CE films can form along air pore walls during the wet fresh mortar stage, right after or even during mixing (Fig. 3d). The latter inference was additionally confirmed by in situ ESEM experiments, where CE also was present at air void interfaces (Fig. 3c).

3.2. Appearance of polymers in the hardened mortar

Depending on their occurrence within the mortar, three different types of polymer domains can be distinguished (Fig. 1): (1) polymer domains at the interfaces between mortar and tile (Fig. 1b) and mortar and substrate, (2) polymer domains at air void interfaces (Fig. 1c), and (3) polymer domains within the cementitious matrix (Fig. 1d). The second type was easily recognised in SEM investigations by its large size and smooth surface. However, in the case of the third and partly also for the first type of polymer films, no morphological criteria are available to properly distinguish them from mineral components because of a dense intergrowth with cement minerals. Therefore, additional criteria, such as density contrast (comparison of BSE and SE images) and the sensibility of polymers to the electron beam (beam damage, as described above), were used for discrimination. Nevertheless, in microstructural investigations, the first and third types of polymer domains are usually underestimated because of the difficulties in identification. Therefore, we focus on the second type of polymer domains at air void interfaces. Based on their characteristic appearance, several film types consisting of different polymer components can be identified.

Fig. 4 shows latex, CE, and PVA structures in non-commercial laboratory mortars modified only with one specific polymer. Although rare, latex films were found, which form thick films (>4 μm) between two adjacent air voids (Fig. 4a). The film edges are rounded. Towards the contact with the matrix, the intergrowth with cement grains gradually increases, creating a rough surface. Pure polymer domains without cement intergrowth generally have a smooth surface, which indicates an advanced latex film formation (Fig. 5a, lower left corner).

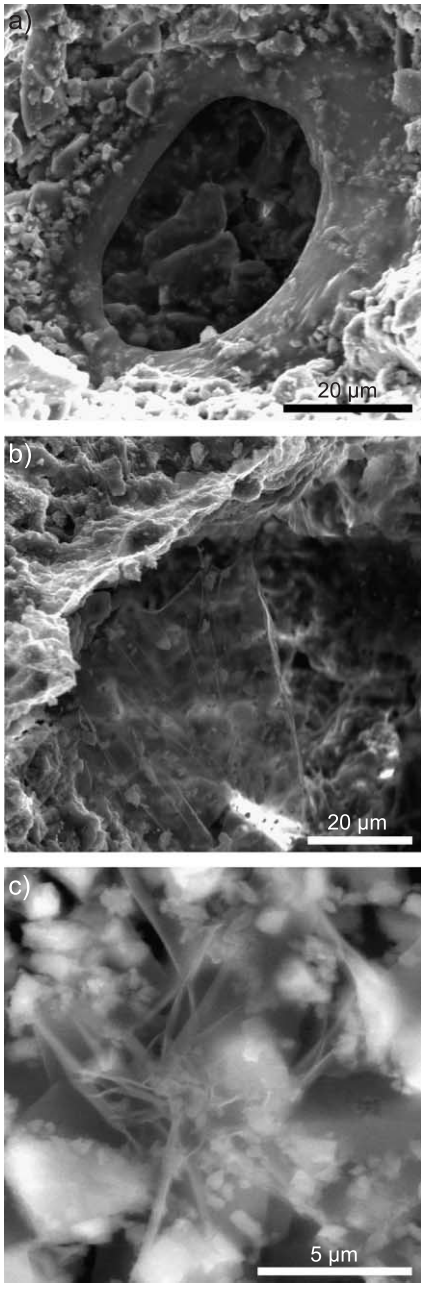

Fig. 4. SEM images of different types of polymeric microstructures on carbon-coated fracture surfaces in model mortars containing only one polymer type: (a) latex, (b) CE, or (c) PVA.

CE films are frequently observed between two juxtaposed air voids and also along the pore wall of a single air void. These sail-like CE films are characterised by a thickness of less than 1 μm. The low thickness and density lead to electron transparency in carbon-coated samples (Fig. 4b). The surfaces of CE films are smooth and cement inclusions are rare.

PVA films closely resemble CE structures with respect to thickness and electron transparency (Fig. 4c). However, PVA domains are rarely observed on the micron scale. Consequently, they are thought to be mainly integrated in the cement–polymer matrix at the submicron scale.

As documented by a comparison between SE and BSE images (Fig. 5a and b), latex films may contain a high quantity of cement minerals. On the SE image, the latex domain appears as a relatively smooth and plain film (Fig. 5a, lower left corner), whereas the BSE image, which reveals more depth information, shows cement minerals that are embedded within the latex film (Fig. 5b). Such massive latex–cement composites are typical for all types of latex films in samples without CE. In real tile adhesive formulations containing both RP and CE, composite structures of the two polymers are frequent, but the resulting composite morphology differs from the massive latex films shown in Figs. 4a and 5a and b. In mortars modified with SA and CE, no electron transparent CE films can be observed. Therefore, the polymer structures are considered to represent CE–latex composites. These composite films are thin and plain (Fig. 5c). Frequent occurrence of fractures as well as sutured edges indicate a brittle behaviour. Again, intense intergrowth with cement phases is documented in the BSE image (Fig. 5d). In mortars modified with EVA and CE, composite polymer structures also differ drastically from pure EVA latex structures. The composite films are thinner, have a plain surface, and are often cracked (Fig. 5e). They partly consist of electron transparent domains, probably composed of pure CE (Fig. 5f). In contrast to samples with SA and CE, the EVA- and CE-modified mortar contains also pure CE films.

In summary, the different polymer components can be distinguished based on distinct morphological characteristics. However, the qualitative identification is mainly restricted to large polymer domains at air void interfaces. To link microstructural information with data from physical tests (e.g., strength), the spatial distribution of different polymer components needs to be quantified, also incorporating small-scale polymer domains within the cement–polymer matrix and/or polymer components at the mortar–tile interface.

3.3. Distribution patterns

Water transport in fresh mortar may lead to a redistribution and fractionation of polymer and mineral components, which can influence final physical properties, such as adhesive strength. Such relationships between microstruc-

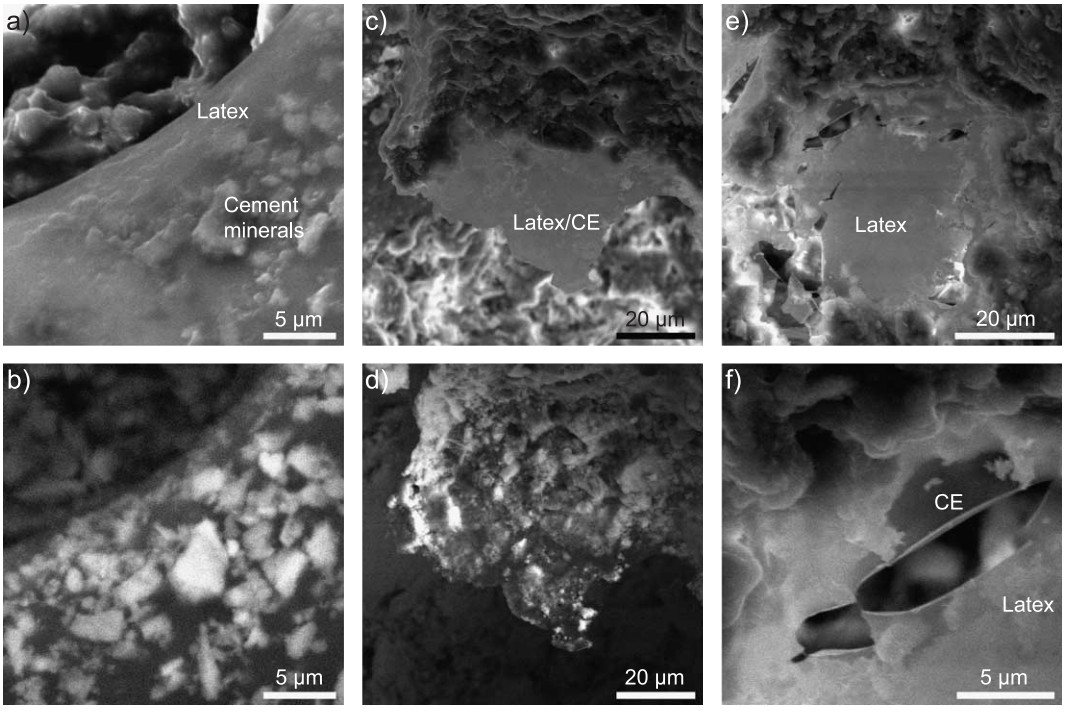

Fig. 5. Composite structures in mortars with several polymer components (SEM images of carbon-coated fracture surfaces). (a) SE and (b) BSE images of VC latex–cement composite microstructures. (c) SE and (d) BSE images of SA latex–CE–cement composite microstructures. SE image of EVA latex intergrown with CE in the overview (e) and a close-up view from the area in the upper left corner (f).

tures and physical properties can be detected by comparing distribution patterns of mortar components with the corresponding failure surfaces.

A representative example for the distribution of VC latex is given in Fig. 6, indicating that within the analytical error, the latex is evenly distributed within the cement–polymer matrix along the *y* axis (Fig. 2). A comparison of measurements performed on former grooves and ripples (application stage) also reveals homogeneous VC latex distribution. In all cases, no latex was measured within the underlying porous concrete substrate or the tile.

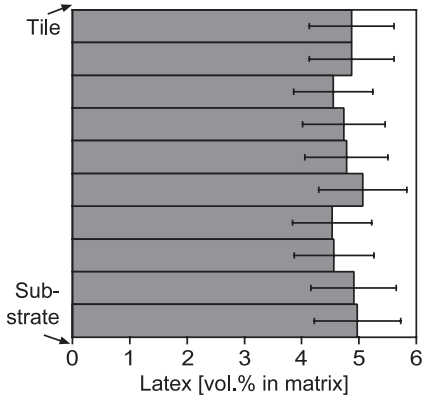

Fig. 6. Concentration profile of VC latex in the cement–polymer matrix sampled across the mortar bed on an *xy* section (Fig. 2). Data is collected by electron microprobe analysis (chlorine distribution map) and then processed with image analysis. The area analysed is 1.5 mm wide and the thickness of the mortar bed is about 1.3 mm. Average concentrations are determined for 10 stripes parallel to the mortar bed. Each stripe represents an area of approximately 1.5×0.13 mm.

Analogously, representative diagrams for the distribution of CE and PVA are shown in Fig. 7. In the case of CE in VC-modified mortar, a slight but continuous increase towards the substrate is observed (Fig. 7a). However, in the lowermost part of the mortar bed, the CE concentrations decrease. Maximum CE concentrations are observed at the top of the first contact layer.

In the SA-modified mortar sample, the CE distribution is more heterogeneous (Fig. 7c). Again, the CE concentrations decrease towards the underlying concrete substrate. In analogy to Fig. 7a, a local maximum occurs at the top of the first contact layer. For all distribution diagrams, a slight but reproducible enrichment of CE is observed directly at the contact between mortar and tile. These results are consistent with Zurbriggen [19], who measured CE enrichments in tile adhesives towards the porous substrate and the porous tile.

In both VC- and SA-modified mortars, PVA is homogeneously distributed in the upper mortar part. Only at the top of the first contact layer a slight, but reproducible enrichment, occurs (Fig. 7b and d). Furthermore, a slight enrichment of PVA exists at the mortar–substrate interface.

About 2% of total CE and 7% of total PVA can penetrate to a maximum distance of 300 µm into the concrete substrate along microcracks. In contrast, latex was never found in the concrete substrate.

In general, the volume fraction of anhydrous cement phases is systematically 0.05 higher for latex- and CE-

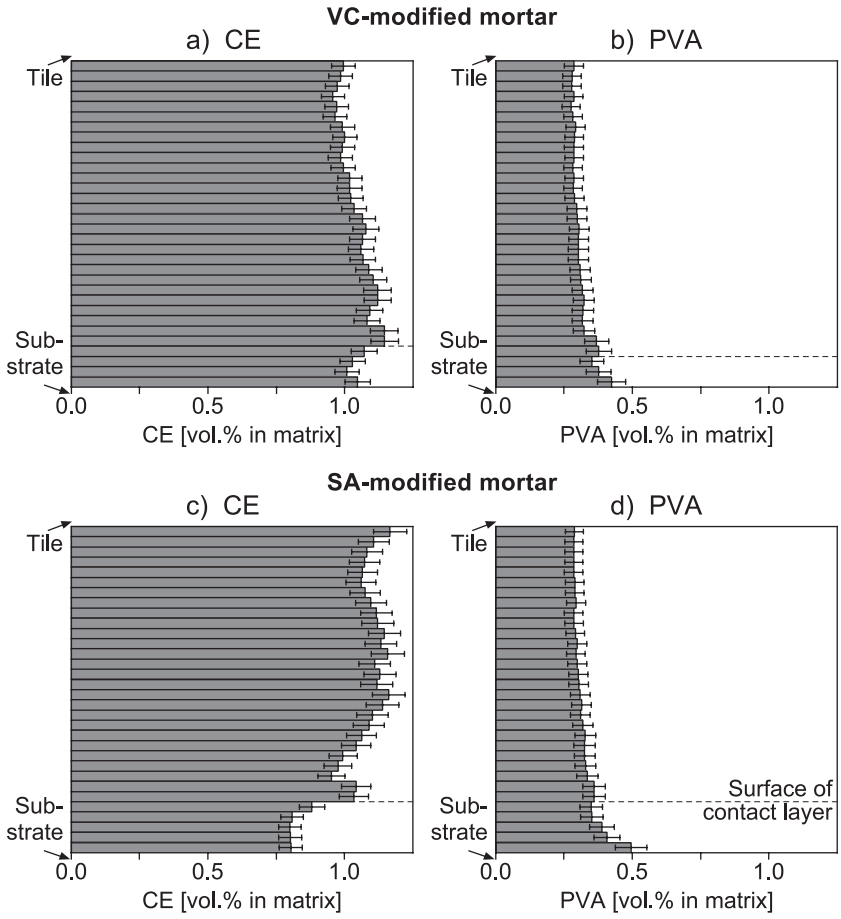

Fig. 7. Concentration variations of CE and PVA in the cement–polymer matrix as a function of the distance from the substrate surface (along *y* axis in Fig. 2). (a, b) VC-modified mortar. (c, d) SA-modified mortar. Data is collected by confocal LSM on an *xy* section (Fig. 2), and then processed with image analysis. The analysis was done over the half length of the mortar bed (along *x* axis, Fig. 2) resulting in an area of 25×1.3 mm.

modified mortars compared to mortars without latex. For all samples, the local variations in the volume fraction of anhydrous phases are smaller than 0.1 and no identical distribution patterns can be observed in different samples. Further differentiation of the cement hydration products by more precise TGA indicates a $Ca(OH)_2$ depletion towards the substrate (Fig. 8).

3.4. Adhesive strength and failure surface analysis

A general relationship of adhesive strength as function of different polymer components (CE, PVA, and several types of latex) is shown in Fig. 9, where six mortar formulations with different polymer components have been tested.

In latex-free samples, the addition of PVA leads to a slight increase of adhesive strength (see also Ref. [31]), while different latex modifications (VC, SA, and EVA) lead to a strong increase in adhesive strength. Note that the measurements of RP-modified mortars are situated within the error range of ±10%. A higher latex concentration clearly increases adhesive strength.

Studies of the failure surfaces document important structural variations, which can be linked with the measured adhesive strength. On the macroscopic scale, adhesion failure occurs more frequently at former mortar ripples, whereas cohesion failure is mostly restricted to former grooves (Fig. 10). Adhesion fractures are exclusively

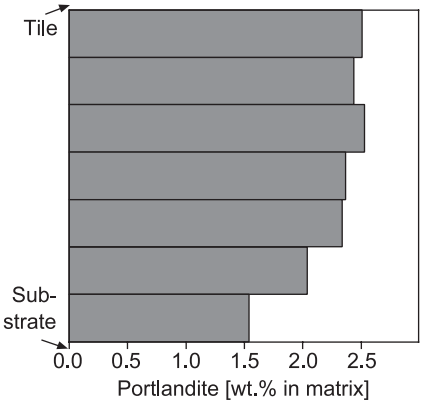

Fig. 8. Distribution diagram of portlandite $Ca(OH)_2$ in mortar as a function of the distance from the substrate surface (*y* axis in Fig. 2). Data are based on TGA bulk analysis of a measurement series sampled across the mortar bed. Each sample corresponds to a layer in the *xz* plane (Fig. 2) of about 0.2 mm thickness. The effect of potential carbonation of $Ca(OH)_2$ during TGA is discussed in the text.

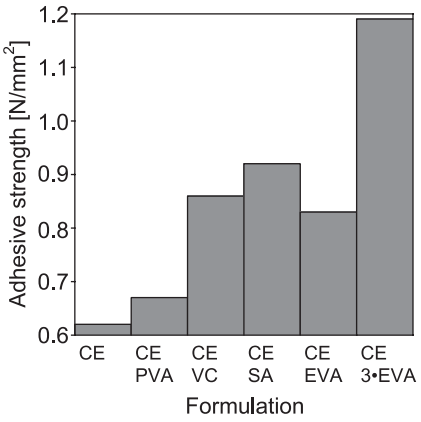

Fig. 9. Adhesive strength of mortars modified with different polymer combination (Table 1). Each of the six data bars represents the average value obtained from five measurements on equivalent samples. The PVA content in formulation "CE/PVA" equals the PVA content in the formulations containing RP ("CE/VC", "CE/SA", "CE/EVA"). The content of RP in formulation "CE/3 · EVA" is 6 wt.%, three times higher than the standard mortar.

localised at the tile–mortar interface. Failure at the mortar–substrate interface is not observed, but cohesion failure occurs at the first contact layer surface. In Fig. 10, the values of the adhesive strength tests are plotted against the area percentages of cohesion fracturing observed on the failure surfaces. All data are collected from the same sample (SA- and CE-modified mortar). The linear trend indicates a positive correlation between area percentage of cohesion failure and adhesive strength.

SEM investigations on failure surfaces point out microstructural differences between former ripples and grooves. The lower part of the inset of Fig. 11 depicts the ripple area with a smooth failure surface (adhesion failure), which shows significantly less air voids than the interior of the mortar bed. Unusually large air voids with irregular shape correspond to air voids, which were entrapped during tile inlaying (arrow in inset of Fig. 11; [22]). The upper part of the inset reflects the area of a former groove region, which is characterised by a low proportion of adhesion fracturing. In

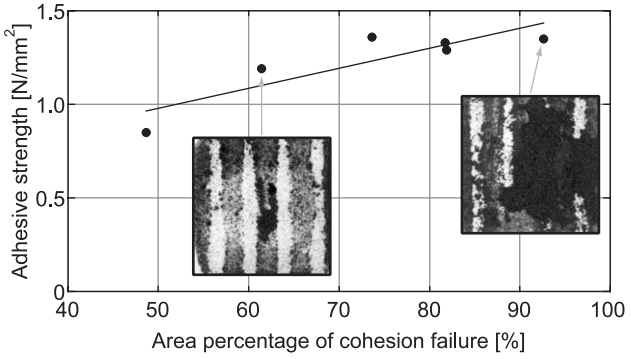

Fig. 10. Adhesive strengths plotted versus the area percentage of cohesion fractures. Data represent six equivalent mortar samples (modified with SA and CE). The two micrographs document the mixed failure patterns on the tile side. The dark and bright areas represent cohesion and adhesion failure, respectively.

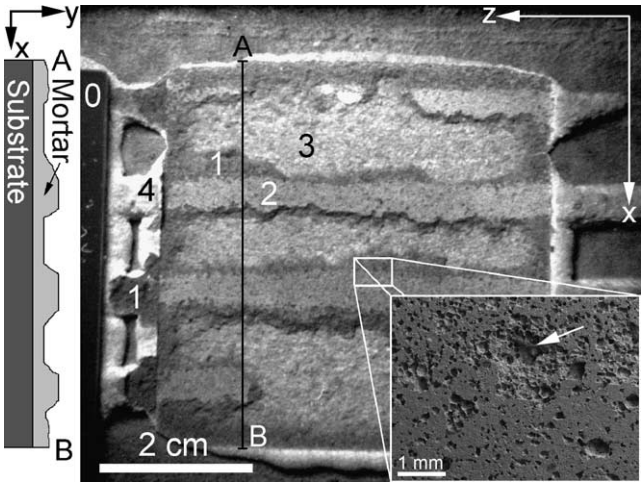

Fig. 11. Top view and schematic profile A–B (trace of profile is indicated in the picture) of a mortar sample illuminated with ultraviolet light to excite the stained CE within the mortar. The relative amounts of CE are represented by different light intensities (increasing from 0 to 4), which correspond with specific mortar domains: 0=tile, 1=cohesion fracture, 2=adhesion fracture at the mortar–tile interface, 3=fracture at the top of the contact layer, and 4=mortar surface beside the tile (not covered). The inset (bottom right) represents an SE SEM image of a failure surface at the ripple–groove transition.

contrast to the ripple domains, the size of air voids in the groove domains is comparable to those in the mortar's interior. Deeper structural domains are exposed due to cohesion failure within the mortar bed.

Based on fluorescence microscopy, CE and PVA distributions on failure surfaces can be monitored. This is shown in Fig. 11 where the brightest domains (4) represent surfaces which were not covered by a tile. The enrichments at the mortar–tile interface and at the contact layer surface (Domains 2 and 3) exposed due to adhesion fracturing are weaker. Darkest areas reflect surfaces of cohesion fractures depleted in CE (1).

4. Discussion

Based on numerous micro- and macroscopic observations, the structural evolution of polymer-modified mortars can be reconstructed. The associated mechanisms, such as film formation, drying due to evaporation, and hydration, are summarised schematically in Fig. 12. Although the mechanisms described below occur in similar applications, the resulting microstructures can change depending on the experimental setup. The following discussion focuses particularly on the role of polymers during the microstructural evolution and their influence on the physical and macroscopic properties of the investigated mortars.

4.1. Mixing

With respect to cement hydration, the mixing time coincides with the so-called induction period, which is

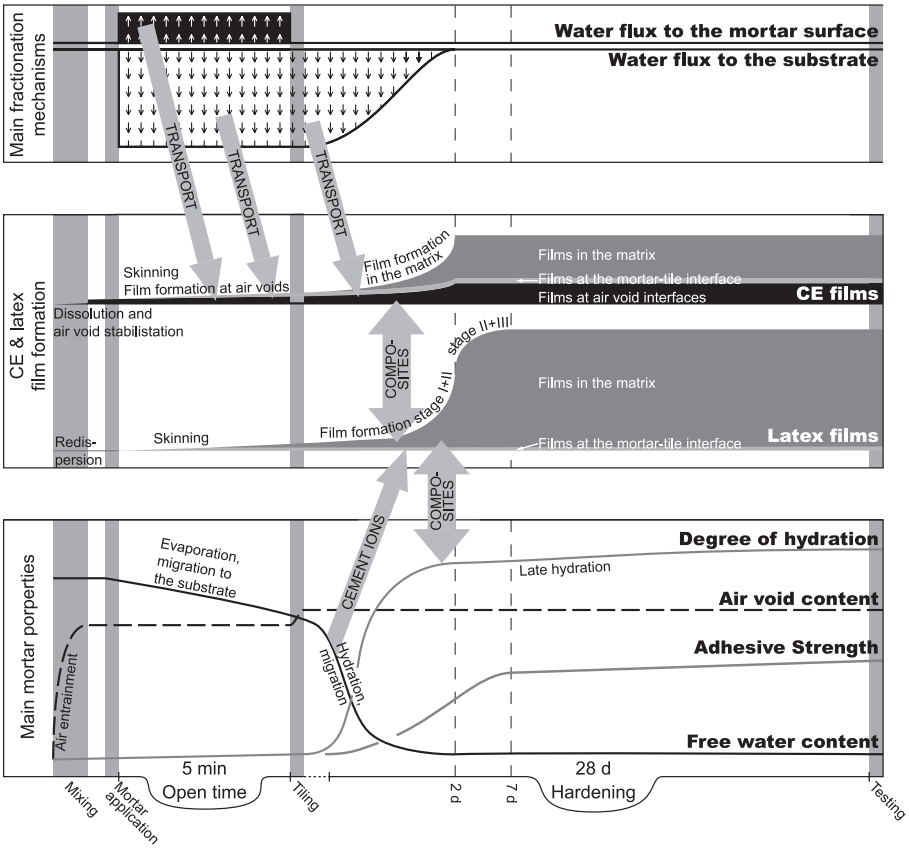

Fig. 12. Schematic synthesis of the mortar evolution. The nonlinear horizontal time axis highlights the major stages of the mortar evolution.

dominated by a rapid exothermal dissolution of ions and the coeval formation of hydrate shells around the anhydrous clinker grains. This process starts immediately after water contact. As a result, the pore solution reaches a high ionic strength and pH values of about 13. A review of hydration processes is given for example in Refs. [32,33].

Simultaneously, several important, polymer-related mechanisms occur: (a) air entrainment, (b) redispersion/dissolution of RP, and (c) initiation of CE film formation.

(a) The air void content of mortars modified exclusively with CE is about 20 vol.%, whereas nonmodified mortars contain only a few volume percent (standard pycnometer measurements). This implies that the air voids entrained during mechanical mixing are stabilised by CE. This is confirmed by ESEM in freeze-dried samples of fresh mortar (Fig. 3c), where the stabilisation is associated with an enrichment of CE at the interface between air void and wet cement paste. This enrichment can be assigned to the properties of CE as surface-active agent with a strong affinity to the gas–water interface. During mechanical mixing, the air voids are moved through the mortar and hence CE, which is dissolved in the pore solution, becomes attached at the air void interface. The air improves the workability during trowelling and tiling by influencing the mortar's rheology and compressibility during the fresh mortar stage.

(b) RP can also influence the mortar's bulk rheology by slight air entrainment, mortar plasticising, and stabilising, and the efficiency of RP with respect to these processes is strongly dependent on its redispersion rate. A homogeneous RP distribution also requires redispersion, and is important to prevent the formation of zones with unfavourable properties in both fresh and hardened mortar. The process of redispersion can be observed in model experiments (Fig. 3a; [25]), where the agglomerates of the RP disperse into the single latex particles. Proper redispersion is driven by the latex-stabilising systems, redispersion aids, and mechanical shearing. Thereby, the unbound part of PVA can separate from the latex and form individual microstructures (PVA films). This separation is assumed to start very early, probably during mixing. With respect to the real mortar, a perfect redispersion of RP in cement pastes is indicated by the homogeneous distribution patterns for latex throughout the cement matrix (Fig. 6).

(c) CE films are observed in fresh pastes (Fig. 3d). This is a clear indication for their formation during the mortar's wet stage, and the film formation driving force must therefore be their surface activity (Fig. 12).

4.2. Mortar application and Open Time

Inhomogeneous phase distributions within the mortar bed and at the mortar–tile interface are partly related to the method of mortar application and the duration of the Open Time (time interval between application of mortar and tiling). The mortar is applied by a toothed trowel to generate an alternating pattern of ripples and grooves, providing a constant thickness of the applied mortar layer. As the toothed trowel runs several times over the contact layer, the positions of the ripples can shift laterally, which may create cavities as observed in Fig. 13b. At this stage, water migration due to evaporation induces mortar fractionation, which invokes compositional gradients within the mortar ripples. Open Time may lead to skinning, which considerably reduces the wettability of the tile by fresh mortar and may reduce adhesion properties. The term skinning describes the sum of all mechanisms that change the composition of the mortar surface during the Open Time. The mobility of polymer components was investigated in case of mortar ripples, which remained uncovered until fully dried and hardened. Fig. 13a shows a strong enrichment of PVA at the interfaces towards both air and substrate, where evaporation and capillary forces in the porous substrate, respectively, induce migration of the pore water and therein dissolved species to these interfaces. A similar transport and accumulation pattern occurs for CE. This accumulation geometry can be complicated by the occurrence of cavities, where an additional enrichment of CE or PVA at the surface of the cavity leads to an internal inhomogeneity, further increasing the CE/PVA concentration on top of the contact layer as the ripple is compressed during tiling (Fig. 13b). In samples with a standard Open Time of 5 min, the enrichment at the mortar–tile interface is small for CE and even below the detection limit for PVA (Fig. 7). Furthermore, dissolved inorganic components are migrating with the pore solution towards the surface and the substrate. However, associated processes, such as cement hydration and capillary transport, towards the substrate persist after the tile inlaying. The distribution patterns of inorganic phases are therefore not exclusively related to the Open Time fractionation and are discussed in relation with the progressive drying during the hardening process. Nevertheless, it is important to note that the enrichment of inorganic phases at the surface may also contribute to skinning. Preliminary measurements revealed an increased concentration of $CaCO_3$ formed during Open Time at the surface. This is explained by portlandite efflorescence immediately followed by fast carbonation. As observed on common failure surfaces (e.g., Fig. 11), mortars predominantly fail along surfaces where skinning occurred. Therefore, these areas represent the weakest zones of the entire mortar bed.

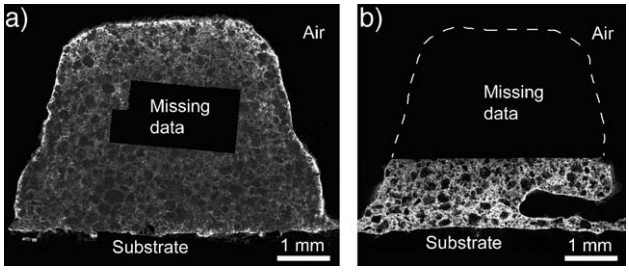

Fig. 13. LSM image showing cross-sections of hardened mortar ripples beside a tile (composition according to Table 1, latex: SA). As no tile covered this mortar, evaporation induced water flux to the mortar surface was active from mortar application until drying was completed. Note that this differs to the standard samples, where this mechanism acts only during the Open Time of 5 min, until the tile is inlayed. CE and PVA enrichments are bright. (a) PVA enrichment at the mortar–substrate interface and at the mortar surface. (b) CE enrichment at the contact with an internal cavity.

4.3. Tiling

The moment of tiling is an important step because the 6-mm-high ripples become squeezed to a continuous mortar bed of 1–2 mm thickness, inducing a considerably mass flow. Particularly, the associated mortar flux was studied in an experiment using a calcite-free mortar formulation, where parts of the ripple and groove surfaces were marked with powdered calcite. The final location of the markers in a cross-section was investigated using optical light microscopy. By comparison of initial and final position of the markers, inferences about the flow pattern in the mortar can be drawn. At the mortar–tile interface, the initial surfaces at the top of the ripples are preserved, whereas the ripple flanks are completely disrupted. In the latter case, some parts are moved towards the tile interface in an area corresponding to a previous groove, while other parts are now embedded within the mortar matrix. In the experiment, the markers can be used to study the mechanical redistribution of the mortar surface previously affected by skinning. As shown in Fig. 14, skins are mainly preserved on top of former ripples and on the bottom of former grooves. This geometry dominates the failure locations (Fig. 11): adhesion fracturing is prevalent at ripple surfaces, whereas cohesion fracturing occurs predominantly in former groove domains (Figs. 10 and 11).

4.4. Hardening

During the hardening process, cement hydration and latex film formation continuously increase the strength of the bulk system. One critical parameter during hardening is the water concentration gradient, which is generated by capillary transport into the concrete substrate, by evaporation at the tile grouts and by chemical drying due to cement hydration. Due to the early drying, the cement hydration can be drastically reduced, and, thus, differs from the degree of hydration of systems without this early loss of water (e.g., Ref. [17]). The water retention ability of CE and the amount of the finest-sized pores retard drying.

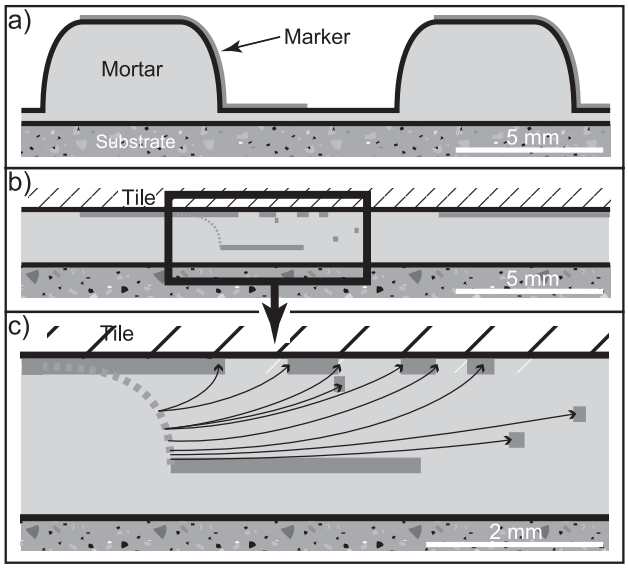

Fig. 14. Simplified diagram showing experiments on mortar flow caused by tile inlaying. (a) Parts of the ripple and groove surfaces have been covered with a marker. (b) After tile inlaying, the markers are redistributed over the mortar layer. (c) Arrows indicate inferred mortar flow during tiling.

The vertical water flux into the underlying substrate results in a redistribution of organic and inorganic components. Figs. 6 and 7 indicate that the mobility is different for each of the three polymer types. PVA concentrations markedly increase towards the substrate. This enrichment can be attributed to a filtering effect associated with carbonation in the uppermost layer of the concrete substrate. Carbonation leads to a general reduction of the pore size preventing the polymers from penetrating the concrete substrate. This is confirmed by the observation that PVA and CE in the substrate are exclusively found within microcracks and not within the cementitious matrix. Analogously, the surface of the contact layer undergoes a pore size reduction due to smoothing by the trowel. Therefore, this horizon filters the downward migrating pore water, generating enrichments of PVA and CE.

In contrast to CE and PVA, latex distribution is homogeneous (Fig. 6) because latex was evenly distributed during mixing, and not transported during later stages. The immobility of latex can be attributed to (a) particle size, (b) adsorption on cement particles, and (c) wet sintering.

(a) Latex particles have a size between 400 nm up to a few microns, whereas the porosity of the C-S-H gel ranges down to 10 nm. Therefore, latex particles are not able to migrate through the capillary pore system.
(b) Stark et al. [14], Su et al. [16], and Dimmig [17] observed styrene acrylate latex adsorption on mineral surfaces, a process which also reduces the mobility of latex.
(c) Routh and Russel [34] describe latex film formation under wet conditions (wet sintering), which reduces latex mobility.

The redistribution of inorganic components due to water migration can barely be detected by means of element distribution mappings in the hardened mortar. Nevertheless, compositional gradients detected by TGA suggest portlandite depletion towards the concrete substrate (Fig. 8). As the drying front is progressing from grout to centre and from substrate to tile, hydration is stopped earlier in the peripheral grout region and near the substrate. In addition to drying, the binding of Ca ions by latex (first proposed by Ref. [2]) can hinder portlandite growth. But this mechanism cannot cause local portlandite depletion, as the latex phase is evenly distributed across the mortar bed. The overall degree of hydration (reflected by the anhydrous volume fraction determined by image analysis of BSE SEM) seems to be uniform from substrate to tile, as this method is less sensitive than TGA profiling. Based on the overall uniform degree of hydration, local strength variations within the mortar bed are not expected. In addition, polymer modification does not induce a significant reduction of the degree of hydration compared to unmodified mortars (measured by TGA and image analysis). Therefore, it is supposed that the hydration slows down due to drying of the thin mortar bed and not due to polymer-induced retarding of hydration as described in Refs. [17,35].

Film formation occurs over an extended period and is also strongly related to the water content. For solution polymers (i.e., CE and PVA), film formation is mainly driven by evaporation. Additionally, adsorption behaviour, surface activity, cross-linking, complexation, coagulation, and reduced solubility are further driving mechanisms for the accumulation of polymers and the formation of films.

More specifically, CE is already present at the air void interfaces during the mixing stage (Fig. 3c and d). Further drying leads to a closer entanglement of the CE chains, and film contraction. In advanced stages, CE films may detach from the air void interface, forming sail-like structures in the void (Fig. 4b).

Compared to CE, PVA is less surface active and therefore, the enrichment at air void interfaces is less effective. In addition, the PVA content in the mortar is generally much lower. Hence, PVA films predominantly occur within the cement–polymer matrix on a submicron scale.

In this context, it is important to note that most of our qualitative observations are restricted to relatively large polymer films at air void interfaces and large capillaries (Figs. 1, 4 and 5). However, small-scale domains within the finer capillaries and the submicron-scaled intergrowth of polymers and minerals in composite microstructures may be even more important for the overall material properties. However, it is suggested that driving forces similar to those described for the larger films would also act at the submicron scale.

The formation of latex films is even more complicated because film formation is based on latex particles and a sequence of different film formation processes. Latex film formation starts with agglomeration (Stage I) and deforma-

tion of these particles into hexagonal shapes (Stage II). Routh and Russel [34] describe a variety of different film formation mechanisms during Stages I and II, which can be used to explain skinning and particle deformation during wet and dry mortar conditions. Four independent arguments lead to the conclusion that latex film formation, at least partly reaches the advanced Stage III of particle coalescence, where polymers diffuse across initial particle boundaries. (1) A major strengthening of latex-modified mortars occurs well after the free water is used up, cement hydration stops and capillary latex deformation mechanisms after Ref. [34] are assumed to slow down significantly (Fig. 12). (2) Latex films in mortars show very smooth surfaces, and relict particle structures are rare (Fig. 5a). (3) Latex films in mortars do not redisperse during water immersion [20,24]. As capillary deformation of the latex particles is principally a reversible mechanism dependent on the humidity, particle coalescence is a possibility to explain the water resistance. (4) Prolonged hot storage at 70 °C or even around 100 °C does not enhance adhesion properties. If, under normal storage conditions, the latex forms films by capillary deformation, only, then increased diffusion rates during hot storage should significantly improve strength properties. As this is not the case, the degree of coalescence might be already high before heat treatment, after normal storage conditions (23 °C/50% RH).

Cement phases and cement ions in the pore water influence the latex film formation [8,24]. These cement–latex interactions induce a strong intergrowth at the submicron scale between the two phases, leading to the formation of the cement–polymer matrix, also described in Refs. [17,35]. As this is the main occurrence of latex in the microstructure, the latex–cement composite matrix is thought to have a major influence on the final properties of latex-modified mortars.

Comparison of latex structures in RP-modified mortars with and without CE indicates that the latex morphology changes (Figs. 4 and 5), pointing to latex–CE interaction. Thus, sail-like CE structures are absent in SA-/CE-modified mortars while they are still present in CE-/VC- and CE-/EVA-modified mortars. Therefore, the latex type influences the CE–latex interaction. Additionally, the difference in the CE distribution patterns between VC-/CE- and SA-/CE-modified mortars suggests an influence of these latex-specific interactions on the CE mobility in the mortar (Fig. 7).

4.5. Adhesive strength and failure modes

Latex modification leads to an improved adhesive strength of the hardened mortar (Fig. 9). Consistently, neither failure surfaces nor fracture surfaces parallel to the *xy* plane in Fig. 2 intersect latex films (Fig. 4a). In contrast, many CE films are fractured (Fig. 4b). Consequently, CE films are weaker than latex structures and contribute less to the total adhesive strength than latex films (also shown by Fig. 9).

A major difference in fracture behaviour is observed in relation to the trowelling pattern of ripples and grooves. Above ripples, the tile contacts a surface that underwent skinning, where adhesion fracturing predominates. In the region of former grooves, mortar flow during tile inlaying forces fresh paste to wet the tile properly, and cohesion fracturing is more frequent (Figs. 10 and 11). This is clear evidence that skinning can drastically reduce adhesion properties.

Entrapped air voids at the mortar–tile interface (inset Fig. 11) are a direct consequence of an uneven mortar surface and a stiff skin, because it prevents entrapped air to be mixed and sheared into the paste while tiling. Instead, the entrapped air remains at the interface with the tile and decreases the contact area between tile and mortar, which again, reduces adhesion properties [22].

To summarise, adhesive strength varies within the same formulation (Fig. 10). However, samples with higher adhesive strength show increased percentages of cohesion fracturing, a correlation that is observed for all latex-modified tile adhesives. Hence, the mortar–tile interface is the weakest element of the substrate–mortar–tile system and therefore dominates failure behaviour.

5. Conclusions

The influence of polymers on microstructure and physical properties of mortars can be described as follows:

- The addition of latex increases adhesive strength of a tile adhesive mortar. Microstructural investigations confirm that latex is dispersed homogeneously in the cement–polymer matrix, which causes an improvement of both final cohesion and adhesion properties.
- Latex films with a width of 10–100 μm are observed at air void interfaces. These films usually include CE as a second polymer component and tend to be intergrown with cement phases. It is assumed that such composite latex–CE films also represent the predominant occurrence of latex in the matrix. Therefore, they are considered to be responsible for the observed increase of adhesive strength. The affinity to form composite latex–CE films and their morphology is dependent on the type of RP latex (SA, EVA, and VC). Further investigations are needed to evaluate the influences of this latex–CE interaction on the mortar properties.
- Both PVA and CE are dissolved in the pore solution and can form isolated films upon drying.
- During the Open Time, evaporation induces a water flux to the surface, whereas capillary forces pull the water to the porous substrate, a process that continues after tiling. The migration of pore water leads to a fractionation of dissolved species, resulting in a distinct enrichment of

PVA and CE above the substrate. With respect to the inorganic components, fractionation associated with water migration leads to a depletion of portlandite towards the mortar–substrate interface.

- Investigation of failure surfaces reveals that mortar–tile interfaces represent the weakest part in the system. The adhesive strength of the entire system is dominated by the properties of this interface. In this context, skinning reduces adhesive strength. For that reason, future developments and research should focus on improvement of the interface properties.

Acknowledgements

Many of the results from this study are based on samples carefully prepared by Dominique Schaub, Verena Jakob, and Jürg Megert. Their assistance is gratefully acknowledged. We would like to thank Robert Koelliker, Karl Ramseyer, and Adrian Pfiffner for valuable discussions. Financial support from KTI for project No. 4551.1 KTS is gratefully acknowledged. The electron microprobe used in this study was financed by Swiss National Science Foundation (Credit 21-26579.89). We greatly acknowledge Hans Imboden for giving us access to the LSM of the Institute of Cell Biology (University Bern).

References

[1] P.K. Mehta, Concrete: Structure, Properties, and Materials, Prentice-Hall, Englewood Cliffs, NJ, USA, 1986.
[2] Y. Ohama, Principle of latex modification and some typical properties of latex-modified mortars and concretes, ACI Mater. J. 84 (6) (1987) 511–518.
[3] Y. Ohama, Handbook of Polymer-Modified Concrete and Mortars, Properties and Process Technology, Noyes Publications, Park Ridge, NJ, USA, 1995.
[4] J. Schulze, Redispersionspulver in Zement, Tonind.-Ztg. 109 (9) (1985) 698–703.
[5] J. Schulze, Influence of water–cement ratio and cement content on the properties of polymer-modified mortars, Cem. Concr. Res. 29 (1999) 909–915.
[6] J. Schulze, O. Killermann, Long-term performance of redispersible powders in mortars, Cem. Concr. Res. 31 (2001) 357–362.
[7] M.U.K. Afridi, Y. Ohama, M.Z. Iqbal, K. Demura, Water retention and adhesion of powdered and aqueous polymer-modified mortars, Cem. Concr. Compos. 17 (1995) 113–118.
[8] J.A. Larbi, J.M.J.M. Bijen, Interaction of polymers with Portland cement during hydration: A study of the chemistry of the pore solution of polymer-modified cement systems, Cem. Concr. Res. 20 (1990) 139–147.
[9] S.A. Rodger, S.A. Brooks, W. Sinclair, G.W. Groves, D.D. Double, High strength cement pastes: Part 2. Reactions during setting, J. Mater. Sci. 20 (1985) 2853–2860.
[10] D.A. Silva, H.R. Roman, P.J.P. Gleize, Evidences of chemical interaction between EVA and hydrating Portland cement, Cem. Concr. Res. 32 (2002) 1383–1390.
[11] S. Chandra, P. Flodin, Interactions of polymers and organic admixtures on Portland cement hydration, Cem. Concr. Res. 17 (1987) 875–890.
[12] D.A. Silva, V.M. John, J.L.D. Ribeiro, H.R. Roman, Pore size distribution of hydrated cement pastes modified with polymers, Cem. Concr. Res. 31 (2001) 1177–1184.
[13] K. Tubbesing, Mikrostruktur von PCC: Gefügeuntersuchungen an polymermodifizierten Zementsteinen, PhD thesis, Technische Universität Hamburg-Harburg, Hamburg, 1993.
[14] J. Stark, A. Dimmig, S. Müller, Interactions between polymer and cement, Beton-Fertigt.-Tech. (11) (2001) 40–49.
[15] Z. Su, Microstructure of polymer cement concrete, PhD thesis, Material Sciences Group, Delft University of Technology, Delft, Netherlands, 1995.
[16] Z. Su, K. Sujata, J.M.J.M. Bijen, H.M. Jennings, A.L.A. Fraaij, The evolution of the microstructure in styrene acrylate polymer-modified cement pastes at the early stage of cement hydration, Adv. Cem. Based Mater. 3 (1996) 87–93.
[17] A. Dimmig, Einflüsse von Polymeren auf die Mikrostruktur und die Dauerhaftigkeit kunststoffmodifizierter Mörtel (PCC), PhD thesis, Bauhaus-Universität, Weimar, 2002.
[18] D. Schweizer, The Role of Cellulose Ethers in Gypsum Machine Plaster, Proc. ConChem., Düsseldorf, 1997, pp. 227–234.
[19] R. Zurbriggen, Investigation of the segregation behaviour of different mortar constituents with TGA/SDTA, in: UserCom (Information for Users of METTLER TOLEDO Thermal Analysis Systems), vol. 13, METTLER TOLEDO, Schwerzenbach, Switzerland, 2001, pp. 9–11.
[20] L. Holzer, A. Jenni, R. Zurbriggen, Eine in-situ ESEM—Studie über mikrostrukturelle Veränderungen polymervergüteter Mörtel während der Wasserlagerung, Proc. 3. Tagung Bauchemie, vol. 24, GDCh-Facharuppe, Frankfurt, Germany, 2001, pp. 156–159.
[21] A. Jenni, M. Herwegh, R. Zurbriggen, L. Holzer, Sample preparation of polymer-modified high-porous mortars for quantitative microfabric analysis, Proc. 8th Euroseminar on Microscopy Applied to Buildings Materials, Athens, Greece, Cosmosware, Agia Paraskevi, Greece, 2001, pp. 571–578.
[22] A. Jenni, M. Herwegh, R. Zurbriggen, T. Aberle, L. Holzer, Quantitative microstructure analysis of polymer-modified mortars, J. Microsc. 212 (2) (2003) 186–196.
[23] R. Zurbriggen, Influence of redispersible powders on shrinkage, hydration behaviour and micro-structure of tile adhesives, Proc. 2. Seminar: Beschichtung und Bauchemie, Kassel, Germany, Vincentz Network, Hannover, Germany, 1998, pp. 47–62.
[24] A. Jenni, M. Herwegh, R. Zurbriggen, L. Holzer, Polymerverfilmung in zementären Systemen, in: Proc. 3. Tagung Bauchemie, vol. 24, GDCh-Facharuppe, Frankfurt, Germany, 2001, pp. 92–97.
[25] R. Zurbriggen, A. Jenni, Lichtmikroskopische in-situ Experimente zur Filmbildung von Polymeren in zementären Systemen, Proc. Tagung Bauchemie, Weimar, 2002.
[26] J.I. Goldstein, D.E. Newbury, P. Echlin, D.C. Joy, A.D. Romig, C.E. Lyman, C. Fiori, E. Lifshin, Scanning Electron Microscopy and X-ray Microanalysis, Plenum Press, New York, 1992.
[27] S. Simmons, E.L. Thomas, The use of transmission electron microscopy to study the blend morphology of starch/poly(ethylene–co-vinyl alcohol) thermoplastics, Polymer 39 (23) (1998) 5587–5599.
[28] K.L. Scrivener, H.H. Patel, P.L. Pratt, L.J. Parrott, Analysis of phases in cement paste using backscattered electron images, methanol adsorption and thermogravimetric analysis, Proc. Microstructural Development During Hydration of Cement, vol. 85, Materials Research Society, Pittsburgh, PA, USA, 1986, pp. 67–76.
[29] R. Kriegel, R. Hellrung, A. Dimmig, Qualitative and quantitative analysis of selected organic additives in hardened concrete by thermal analysis and infrared spectroscopy, Proc. 11th International Congress on the Chemistry of Cement ICCC, Durban, Rep. of South Africa, 2003.
[30] H.F.W. Taylor, Cement Chemistry, Thomas Telford Publishing, London, 1997.
[31] J.H. Kim, R.E. Robertson, Effects of polyvinyl alcohol on aggregate-paste bond strength and the interfacial transition zone, Adv. Cem. Based Mater. 8 (1998) 66–76.

[32] L. Holzer, F. Winnefeld, R. Kägi, D. Zampini, Towards an integral understanding of the early cement hydration—A multi-method approach, Proc. 11th International Congress on the Chemistry of Cement ICCC, Durban, Rep. of South Africa, 2003.
[33] J. Stark, B. Möser, A. Eckart, Neue Aspekte der Zementhydratation, in: Proc. 14. Internationale Baustofftagung ibausil, vol. 1, Bauhaus-Universitat Weimar, D-99421 Weimar, Germany, 2000, pp. 1093–1109.
[34] A.F. Routh, B.R. Russel, A process model for latex film formation: limiting regimes for individual driving forces, Langmuir 15 (1999) 7762–7773.
[35] A. Beeldens, D. van Gemert, Y. Ohama, Integrated model of structure formation in polymer modified concrete, Proc. 11th International Congress on the Chemistry of Cement ICCC, Durban, Rep. of South Africa, 2003.